

2 μm Narrow-band Adaptive Optics Imaging in the Arches Cluster

R. D. Blum¹

Cerro Tololo Interamerican Observatory, Casilla 603, La Serena, Chile
rblum@noao.edu

D. Schaerer¹

Laboratoire d'Astrophysique, Observatoire Midi-Pyrénées, 14 Av. E. Belin F-31400, Toulouse, France
schaerer@ast.obs-mip.fr

A. Pasquali

ESO/Space Telescope European Coordinating Facility, Karl-Schwarzschild-Strasse 2, D-85748 Garching bei Munchen, Germany
apasqual@eso.org

M. Heydari-Malayeri

DEMIRM, Observatoire de Paris, 61 Avenue de l'Observatoire, F-75014 Paris, France
heydari@obspm.fr

P. S. Conti

JILA, University of Colorado
Campus Box 440, Boulder, CO, 80309, USA
pconti@jila.colorado.edu

W. Schmutz

Physikalisch-Meteorologisches Observatorium, 7260 Davos, Switzerland
wschmutz@pmodwrc.ch

ABSTRACT

Canada–France–Hawaii–Telescope adaptive optics bonnette images through narrow-band filters in the K –band are presented for the Arches cluster. Continuum fluxes, line fluxes, and equivalent widths are derived from high angular resolution images, some near diffraction limited, for the well known massive stars in the Arches cluster. Images

¹Visiting Astronomer, Canada–France–Hawaii–Telescope, operated by the National Research Council of Canada, the Centre National de la Recherche Scientifique de France, and the University of Hawaii

were obtained in the lines of He I 2.06 μm , H I Br γ (2.17 μm), and He II 2.19 μm as well as continuum positions at 2.03 μm , 2.14 μm , and 2.26 μm . In addition, fluxes are presented for H I P α (1.87 μm) and a nearby continuum position (1.90 μm) from Hubble Space Telescope archival data¹. The 2 μm and P α data reveal two new emission–line stars and three fainter candidate emission–line objects. Indications for a spectral change of one object between earlier observations in 1992/1993 and our data from 1999 are found. The ratio of He II 2.19 μm to Br γ emission exhibits a narrow distribution among the stars, suggesting a narrow evolutionary spread centered predominantly on spectral types O4 If or Wolf-Rayet stars of the WN7 sub–type. From the approximate spectral types of the identified emission–line stars and comparisons with evolutionary models we infer a cluster age between ~ 2 and 4.5 Myr.

Subject headings: instrumentation: adaptive optics — Galaxy: center — stars: early–type — stars: Wolf–Rayet

1. INTRODUCTION

The Arches cluster is thought to be the most massive, dense, star forming cluster in the Galaxy (Serabyn et al. 1998; Figer et al. 1999). This prolific starbursting cluster which may harbor more than one hundred O–type stars (Serabyn et al. 1998) and whose linear size at 8 kpc is only about 0.6 pc in diameter (Figer et al. 1999) was first found in limited near infrared surveys by Nagata et al. (1995) and Cotera et al. (1996). Nagata et al. (1995) named it “Object 17,” for such it was in their spectroscopic survey near the Galactic center. Cotera et al. (1996) referred to the cluster as G0.12+0.2 after its position on the sky, but the cluster has become known as the “Arches” taking the name of the Galactic center thermal Arched Filaments, thermal emission structures 30 pc in projection from the Galactic center (Morris & Yusef-Zadeh 1985). The Arches cluster is located at $\alpha(2000) = 17^{\text{h}}45^{\text{m}}50.^{\text{s}}4$ $\delta(2000) = -28^{\circ}49'22''$ (Figer et al. 1999).

Nagata et al. (1995) presented modest angular resolution images of the Arches cluster, and Cotera et al. (1996) presented low resolution K –band spectra for 13 of the Arches cluster’s brightest stars. Both investigations showed the Arches cluster contained massive emission–line stars similar to those which had been discovered previously in the Galactic center (Forrest et al. 1987; Allen et al. 1990; Krabbe et al. 1991). Figer et al. (1999) used Hubble Space Telescope (HST)/NICMOS images to explore the mass function in the Arches cluster. They found that the Arches cluster IMF is weighted much more to massive stars than “typical” mass functions, e.g. Salpeter (1955). It has been argued that massive stars might preferentially form near the center of the Galaxy due to

¹Based on observations made with the NASA/ESA Hubble Space Telescope, obtained from the data archive at the Space Telescope Science Institute. STScI is operated by the Association of Universities for Research in Astronomy, Inc. under NASA contract NAS 5-26555.”

the pre-conditions there (Morris & Serabyn 1996). The mass function in the Arches cluster thus stands in stark contrast to the OB associations in the Galaxy and Large Magellanic Cloud (Massey & Hunter 1998, LMC), including the massive star cluster R136 in the LMC.

Though there is ample evidence that the Arches cluster harbors a dense cluster of massive stars, and the brightest are apparently evolved as evidenced by their their emission–line spectra (Cotera et al. 1996), the precise mass scale has yet to be set by detailed models of the stars or comparison to evolutionary tracks of stellar parameters determined from spectroscopic measurements. In this paper, we present high angular resolution $2\ \mu\text{m}$ narrow–band images (which cover $36''$ in a single frame) taken at the Canada–France–Hawaii–Telescope (CFHT) and $1.9\ \mu\text{m}$ (archival) images taken with the Hubble Space Telescope (HST)/NICMOS. This is the first of two papers in which we will explore the massive stars in the Arches cluster. Here we present our data and observational measurements. In a subsequent paper we will use the accurate line and continuum fluxes determined from these high angular resolution observations to interpret stellar models and further quantify the properties of the Arches cluster emission–line stars.

2. OBSERVATIONS AND DATA REDUCTION

2.1. CFHT Adaptive Optics Images

The Canada–France–Hawaii–Telescope (CFHT) images were obtained on the nights of 29 and 30 June 1999 and 01 July 1999 using the facility infrared imager, KIR, and the adaptive optics bonnette (AOB), PUEO. KIR employs a 1024×1024 HgCdTe HAWAII detector with $0.035''$ pixels ($36''$ FOV). KIR and PUEO are fully described by Beuzit & Hainaut (1998); see also Rigaut et al. (1998). The Arches cluster data were obtained on 01 July, while observations of Wolf–Rayet (WR) stars and photometric standards were obtained on all three nights. All data obtained on the Arches, WR stars, and standards were obtained with the adaptive optics (AO) corrections on.

Emission–line images were taken through narrow–band filters centered at $2.183\ \mu\text{m}$ (He II, a red-shifted $\text{Br}\gamma$ filter, $\Delta\lambda \approx 300\ \text{\AA}$), $2.17\ \mu\text{m}$ ($\text{Br}\gamma$, $\Delta\lambda \approx 200\ \text{\AA}$), $2.06\ \mu\text{m}$ (He I, $\Delta\lambda \approx 280\ \text{\AA}$). Continuum images were obtained at $2.26\ \mu\text{m}$ ($\Delta\lambda \approx 600\ \text{\AA}$), $2.14\ \mu\text{m}$ ($\Delta\lambda \approx 300\ \text{\AA}$), and $2.03\ \mu\text{m}$ ($\Delta\lambda \approx 210\ \text{\AA}$).

2.1.1. Basic Reduction and Standard Stars

All basic data reduction was accomplished using IRAF³. Each image was flat–fielded using dome flats and then sky subtracted using a median combined image of five to six frames. For the Arches itself, independent sky frames were obtained ~ 19 arcminutes south–east of the cluster.

³IRAF is distributed by the National Optical Astronomy Observatories.

Wolf–Rayet and standard stars used the median combination of the data for sky.

Each night three standard stars were observed. Two of the standards were chosen to span a large range of airmass (approximately one to two airmasses) and observed sequentially over a short time interval. The set of three standards also spanned the observing period of the Arches cluster. The Arches data and Wolf–Rayet stars have been placed on a flux basis by interpolating over the standard star observations as a function of airmass.

The standard stars observed are all early A–type stars: HD130163 (A0V), HD201941 (A2), and HD205772 (A5IV/V). The standard star narrow–band magnitudes were placed on a flux scale by adopting the $2.2 \mu\text{m}$ flux corresponding to the K –band magnitude (Elias et al. 1982) and assuming the relative flux at the filter effective wavelength is given by a 9800 K black body Johnson (1966). The flux at $2.2 \mu\text{m}$ is for α Lyra, $4.07 \times 10^{-10} \text{ W}\cdot\text{m}^{-2}\cdot\mu\text{m}^{-1}$ Tokunaga (1986). On any given night, the difference between the standard star instrumental magnitudes and the assigned flux was less than 5% for all stars observed at similar airmass in all filters. Typically, the difference was about 3% rms. The derived airmass corrections varied between about 0.01 and 0.10 magnitudes per airmass depending on the filter. The $2.03 \mu\text{m}$ and $2.06 \mu\text{m}$ filters showed the largest corrections (0.07 mag and 0.10 mag per airmass) as is expected since this is where the opacity in the Earth’s atmosphere is strongly affected by H_2O and CO_2 molecules.

The resulting point spread functions (PSF) on the final combined CFHT images exhibit full widths at half maximum (FWHM) intensity between 4.9 (the $2.19 \mu\text{m}$ image) pixels to 8.0 pixels (the $2.26 \mu\text{m}$ image). The typical image quality for any of the six final images was thus $0.17''$ to $0.28''$ FWHM. The best image quality was obtained on the $2.19 \mu\text{m}$ image where the airy diffraction pattern can be seen. The minimum airmass for any of the Arches images was 1.5 and some of the images were obtained at 2.0 airmasses, the AOB delivering excellent correction even at such high zenith distance. Several of the standard stars observed near zenith were very nearly diffraction limited. For example observations of WR138 on 30 June were 3.5 pixels ($0.123''$, $\lambda/D = 0.125''$) FWHM in all six filters. Typical estimates of the seeing at V during our run were near $0.8''$ with occasional periods as good as $0.4''$ or as bad as $1.1''$. However, the $2 \mu\text{m}$ images for bright standards or WR stars typically showed FWHMs near the diffraction limit even at airmass up to 2.0 if the seeing at V was better than $\sim 1''$.

2.1.2. DAOPHOT Analysis

The instrumental magnitudes for the Arches data were obtained using DAOPHOT Stetson (1987). The version of DAOPHOT employed is included as part of the XVISTA package V6.0 (Holtzman 2001). The data were analyzed using average PSFs made from four to five stars in the least crowded regions from around the frame. The Arches and WR star images were calibrated using aperture corrections derived from the standard star data and apertures of between 100 and 130 pixels in radius ($7.0''$ to $9.1''$ diameter). Such large apertures were required to obtain all

the flux in the AO corrected images. Aperture measurements were made on the Arches data for the PSF stars after having subtracted the remainder of the stars found by DAOPHOT. Since the brighter PSF stars were located outside the dense core of the cluster, this procedure results in aperture corrections with uncertainties less than three percent in the mean. The total uncertainties in the Arches narrow-band magnitudes are the sum in quadrature of the PSF fitting errors and the uncertainty in the aperture corrections used to put the instrumental magnitudes on a flux scale. The aperture correction uncertainty dominates for the brighter stars and is ± 0.014 , 0.016 , 0.012 , 0.025 , 0.025 , and 0.019 for the $2.26 \mu\text{m}$, $2.19 \mu\text{m}$, $2.17 \mu\text{m}$, $2.14 \mu\text{m}$, $2.06 \mu\text{m}$, and $2.03 \mu\text{m}$ filters, respectively.

The PSF fitting photometry was conservatively limited by considering only stars with uncertainties of 0.2 mag or less since the main goal of this work is to study the brightest emission-line stars at high angular resolution. This resulted in some $\gtrsim 800$ stars in each filter which were subsequently used to construct narrow-band indices (each index is constructed from three filters: one line and two continuum). Further constraining each narrow-band index to have an uncertainty less than ± 0.2 mag and that stars must match to within one pixel from filter to filter, resulted in approximately 550 stars for each narrow-band filter (and thus, in each narrow-band index which requires three magnitudes to derive it; see below) The faintest stars for which narrow-band indices are presented reach a $2.2 \mu\text{m}$ continuum magnitude of approximately 17. The level of completeness is much brighter, especially in the cluster center.

2.1.3. Comparison of WR Star Line Strengths to Spectroscopy

In order to assess the narrow-band filter behavior, WR stars with strong emission lines in He I, Br γ , and He II were also observed and line strengths derived compared to literature values based on spectroscopic measurements. The results are shown in Table 1. Values for equivalent widths (W_λ) from spectroscopic measurements are from Blum et al. (1995a), Crowther & Smith (1996), and Figer et al. (1997). The W_λ (line flux/continuum flux density) for the narrow-band measurements is derived directly from the narrow-band index which is defined as $\text{index} = (f_{\text{line}} - f_{\text{cont}})/f_{\text{cont}}$ where f_{line} is the flux density in the narrow-band passband at the line position, and f_{cont} is the continuum flux density interpolated from the blue and red continuum points nearest to the line. The W_λ follows by multiplication by the appropriate emission-line filter band width, here taken to be the quoted value above for each filter. The index as defined here is a fraction of the continuum.

For the He I line, the stars WR122, and WR123 were observed. WR122 has a very strong He I $2.06 \mu\text{m}$ line and this was found to contaminate the $2.03 \mu\text{m}$ filter (the CFHT $2.03 \mu\text{m}$ filter curve suggests the response is a few % at $2.06 \mu\text{m}$), resulting in a continuum which was too high, hence a line strength which was too low (424 \AA compared to an average value in the literature of 680 \AA ; see Table 1). WR122 is reddened so its continuum is nearly flat at $2 \mu\text{m}$ (Figer et al. 1997). Using only the $2.14 \mu\text{m}$ line as a continuum (which is further separated from the He I line than the $2.03 \mu\text{m}$ filter), the line strength of WR122 is in good agreement with the literature values (623

Å compared to 680 Å). For WR123, the 2.03 μm continuum point is affected by He II emission, and the He I 2.06 μm line itself has both an emission and absorption (P Cygni) component (Figer et al. 1997). The line strength is thus again underestimated. Using only the 2.14 μm continuum point, the narrow-band line strength is within $\sim 40\%$ of the published values, which appears consistent with the observed emission plus absorption components. These potential problems with the He I 2.06 μm line are not important in the present case as we find no evidence for any strong lined He I emission-line stars in the Arches cluster.

The line strength results are more straightforward for $\text{Br}\gamma$, and as Table 1 indicates in good agreement with the literature. A $\text{Br}\gamma$ measurement was obtained for each of WR122, WR123, WR128, WR131, WR134, and WR138. The mean difference (as a percentage of the literature value) is $+0.07\% \pm 0.08\%$. While consistent with no difference, we have made an 0.07 magnitude adjustment to the calibration for $\text{Br}\gamma$ since this value is consistent with the expectation that we have under corrected the standards due to intrinsic $\text{Br}\gamma$ absorption and so over corrected the WR stars. The sense and magnitude of this correction is in good agreement with that found (by different means) by Blum & Daminieli (1999) for similar narrow-band observations.

The measurements for He II are also in good agreement with the literature, with the exception of WR131 (no measurement was made for WR122). Our narrow-band W_λ for WR131 is an order of magnitude brighter than the spectroscopic value given by Figer et al. (1997). There is no obvious reason why such a strong value should be measured, except for the possibility that the line has indeed varied. van der Hucht (2001) have noted that WR131 has "diluted emission lines", which we speculate may be due to the presence of a companion. If the dilution is due to continuum emission from the companion, then the emission lines might vary during an eclipse, but *both* the $\text{Br}\gamma$ and He II lines should vary if this were the case. In anycase, WR131 is a good candidate for future synoptic observations.

2.2. HST NICMOS Images

The $\text{P}\alpha$ (F187N, $\Delta\lambda \sim 190 \text{ \AA}$) and 1.90 (F190N, $\Delta\lambda \sim 190 \text{ \AA}$) μm continuum images were obtained from the HST archive. These images were processed by the standard calnica and calnicb pipelines from the Space Telescope Science Institute (STScI). The images have a total of 256 seconds exposure time each, and the platescale is $0.076'' \text{ pix}^{-1}$. Broad-band images from the same HST program were presented for the Arches by Figer et al. (1999).

Instrumental magnitudes were obtained by DAOPHOT in the same way as for the CFHT data described above. The photometry was calibrated using aperture corrections derived from six pixel radius apertures ($0.9''$ diameter) and the flux calibration of Rieke (2001). The precise values used were 4.107×10^{-5} and $4.455 \times 10^{-5} \text{ Jy-ADU}^{-1}\text{-s}^{-1}$, respectively for the F187N and F190 filters. Zero points for the two filters are 825 and 808 Jy (Rieke 2001). The HST and CFHT magnitudes are not on the same photometric system, but the line and continuum fluxes are, of course, directly

comparable.

The NICMOS data were limited by photometric error in the same way as described above for the CFHT data. This resulted in about 220 stars in each filter and some 200 stars with a $P\alpha$ emission-line index. In principle, the narrow-band index results in an W_λ as determined above for the CFHT data, but here the continuum value is taken directly from the 1.90 μm filter. The faintest stars for which a $P\alpha$ index is presented reach about 16 mag.

3. RESULTS and DISCUSSION

Representative images in the lines of He II (2.19 μm) and $P\alpha$ are shown in Figure 1a and 1b, respectively. The other line and continuum images are not shown (except 2.26 μm ; see below) but are similar. Positions (offsets from the AO guide star; see Figure 1a) for the brightest stars with narrow-band magnitudes in all eight filters (hence four emission line measurements with one exception discussed below) are given in Table 2. We have arbitrarily cut this list at a 2.26 μm magnitude limit of approximately 12 magnitudes (see Table 3). The complete photometry set is available upon request from the authors.

3.1. Narrow-band Indices

In Figures 2, 3, 4, and 5 the narrow-band index is plotted for each emission line. Inspection of the plots suggests the absolute and relative fluxes are quite good: typical stars have very nearly zero line flux (a zero index). The rms deviation (excluding 3 sigma outliers to a linear fit) is 5, 6, 5, and 3 % for the He II 2.19 μm , $\text{Br}\gamma$ 2.17 μm , He I 2.06 μm , and $P\alpha$ 1.87 μm indices, respectively. For the CFHT data, crowding clearly begins to dominate the indices (i.e. the photometry) between 14th and 15th magnitudes.

There are small, systematic, offsets from zero evident in the plots. Such offsets could be due to the intrinsic absorption in the atmospheres of the Arches cluster hot stars, or due to unaccounted for offsets in one or more filters. As described in the following, the most likely case is the latter; however, the knowledge of the expected strength of these features in O and B stars (Hanson et al. 1996) can be used to correct the mean indices. The mean index between 12th and 14th magnitude for the He II 2.19 μm , $\text{Br}\gamma$ 2.17 μm , and He I 2.06 μm indices is -3 , -6 , and -2 %, respectively. The $P\alpha$ 1.87 μm index is approximately zero near 12.5 magnitudes and falls to a minimum of approximately -12% at fainter magnitudes. The $P\alpha$ line index is discussed below; here we concentrate on the 2 μm indices. Main sequence O-type stars exhibit absorption in each of the 2 μm features (Hanson et al. 1996) discussed here, so negative indices might be expected. At 14th magnitude, these objects should be mid to late O, or perhaps early B-type stars (Serabyn et al. 1998). The absorption strengths for such objects are relatively constant for all three features in this spectral type range (Hanson et al. 1996), so we can use the known properties of such stars

to verify or set the mean level of the index in each feature for the Arches cluster stars. From the data presented by Hanson et al. (1996), an estimate of the mean absorption is 1, 4, and 2 $\text{\AA}W_\lambda$ for the He II 2.19 μm , Br γ , and He I 2.06 μm lines, respectively. This translates to index strengths of 0.003, 0.02, and 0.007. This is less absorption than the mean indices imply. Therefore, the indices for each of the 2 μm features have been corrected to these mean values; i.e. the amount of *absorption* in the He II 2.19 μm , Br γ 2.17 μm , and He I 2.06 μm indices has been *reduced* by a constant amount equal to 3, 4, and 2 % respectively in the final determination of the line fluxes shown in Table 4 (the indices in Figures 2, 3, and 4 are the uncorrected, values).

The offset for the P α index is somewhat larger, -12% . By analogy to the Br γ index, systematic absorption at P α 1.87 μm is expected. However, the situation is not as straight forward since there is no blueward continuum point: part of the systematic negative offset seen in Figure 5 might be due to reddening. For heavily reddened objects toward the Galactic center, the continuum actually increases to the red, even for these hot stars. The ratio of blackbody fluxes on the Rayleigh–Jeans tail at 1.87 and 1.90 μm results in an index of $\sim -5\%$ for an interstellar extinction of $A_K = 3.1$ mag appropriate to the Arches (Figer et al. 1999) and using a typical interstellar extinction curve (Mathis 1990). Furthermore, to our knowledge, no study of the intrinsic P α absorption in O and B stars exists. Due to the uncertain contribution to the index from these systematic effects, no correction similar to those for the 2 μm indices has been made to the P α index.

3.2. The Emission–line Stars

The present data set was obtained chiefly to provide better spatial resolution, and hence more accurate line and continuum measurements, for the bright emission–line stars previously discovered in the Arches cluster by Cotera et al. (1996). A graphical demonstration of the improvement obtained by AO and/or HST imaging is shown in Figures 6 and 7. Each individual emission–line object is well separated from the others as (well as with the other non-emission–line sources). This was not the case in images presented by Nagata et al. (1995) and Cotera et al. (1996). These are continuum subtracted line images. For simplicity, the Br γ image is constructed using only the red continuum. Both of these images show that continuum variations can produce spurious emission–line objects; the AO guide star appears due to its strong blue continuum. Our technique of using two continuum filters avoids this problem in general. The AO guide star is also obviously a foreground object based on color and a K –band spectrum (Cotera et al. 1996). The HST PSF and pointing are remarkably stable. The P α image does not show the effects of seeing and scale variations as the ground–based image does.

The set of emission–line stars identified by Nagata et al. (1995) and Cotera et al. (1996) can be easily recognized in Figures 6 and 7. The Cotera and Nagata IDs are given in Table 4. The positions of all the objects presented in Table 4 are marked on the 2.26 μm continuum image (Figure 8).

Comparing the present line fluxes to Cotera et al. (1996), we find a difference of $-30 \pm 70\%$ in the $\text{Br}\gamma$ line. For the stars most isolated (Cotera ID: 1, 9, 10, 11, 13) the fluxes presented by Cotera et al. (1996) are in better agreement with those determined here (Table 4). The RMS difference is $11 \pm 33\%$. Much of this difference is due to Cotera star 11 which is different by a factor of two (more flux in the present data). Considering stars 1, 9, 10, and 13, the fluxes agree to $0 \pm 26\%$. Nagata et al. (1995) present $\text{Br}\gamma$ and $\text{Br}\alpha$ fluxes for eight of the 13 Cotera stars. Their lower angular resolution measurements are also generally in good agreement with our $\text{Br}\gamma$ fluxes. We find a difference of $-40 \pm 50\%$, which reduces to $-20 \pm 20\%$ if we disregard Cotera star 13 in the comparison which is different to our measurement by a factor of 2.

For the remainder of the Cotera et al. (1996) $\text{Br}\gamma$ measurements, there are three objects which differ in flux by a factor of two to three, in each case the Cotera flux being larger, and these are three of the four stars with the largest fluxes reported by Cotera et al. (1996), Cotera stars 2, 3, and 6. The Nagata et al. (1995) values for these objects are actually more consistent with our measurements. The Cotera et al. (1996) spectra were extracted using relatively large sky offsets. It is possible that there is nebular $\text{Br}\gamma$ emission contaminating their spectra. The sky values for each of the filters presented here were determined “locally” as a free parameter in the DAOPHOT PSF fits. It is not clear whether or not local sky values were determined by Nagata et al. (1995).

Cotera et al. (1996) present He II measurements for their stars 2 and 3. Our measurements are in good agreement with those of Cotera et al. (1996), 7.0 ± 2 , and $2 \pm 1 \text{ W-cm}^{-2} \times 10^{21}$ compared to 5 ± 2 and $1.2 \pm 1.6 \text{ W-cm}^{-2} \times 10^{21}$. Cotera et al. (1996) do not present a He II measure for their star 6, though their spectrum clearly indicates He II is present. The level appears similar to that for their star 2, and this is in agreement with our measurements (Table 4). We also find a similar high value for He II for Cotera star 11. The Cotera et al. (1996) spectrum is convincingly devoid of He II, and this is the same object discussed above for which the present data showed a large ($\times 2$) increase in $\text{Br}\gamma$ flux relative to Cotera et al. (1996), suggesting a real change in the atmosphere of this star. Table 4 and Figure 2 both indicate there are a number of other stars with weak, but measurable He II emission. This is particularly evident in Figure 2 where the “scatter” in the brightest stars increases compared to that for the intermediate brightness objects. This effect is not seen in the He I data (Figure 4), suggesting that weak He I $2.06 \mu\text{m}$ emission is generally absent in the emission-line stars consistent with Cotera et al. (1996) and Nagata et al. (1995).

Figures 6 and 7 clearly show a new emission-line star (22 in Table 4) $12.9''$ SE of the AO guide star. The detailed photometry (Table 4) confirms this. This object is south of the region presented by Cotera et al. (1996), and so was not seen in their spectroscopic survey of the cluster. This object was noted in broad-band images by Nagata et al. (1995, their object 9), but they did not explicitly include it as an emission-line star nor did they present flux measurements for it in any emission-line. A number of other, fainter, objects present themselves as candidate emission-line objects in Table 4. Number 19 has a one sigma He II line, a two sigma $\text{Br}\gamma$ line and a 20 sigma $\text{P}\alpha$ line. Stars 8, 16, and 29 are somewhat more marginal detections, primarily based on $\text{P}\alpha$. These are three of the four objects between 11.8 and 12.6 magnitudes in Figure 5 with indices between 10

and 20%; the fourth is star 30. These objects are not blue, which could otherwise lead to a false $P\alpha$ detection. Several objects, such as numbers 20 and 31, have weak $P\alpha$ indicated, but these appear at a level which is not significant compared to the uncertainties in the data (see §3.1). Numbers 19 and 22, as relatively firm detections, are labeled “New” in Table 4; 8, 16, and 20 are labeled as “Candidate.”

There are several yet fainter objects indicated as emission–line objects in Figures 2, 3, 4, and 5. For the ground–based data, many of these are probably actually due to effects related to point source crowding on the stellar photometry and follow–up spectroscopy might be performed to confirm their nature.

3.3. Spectral Types of the Emission–line Stars and the Age of the Arches Cluster

The line strength information for the Arches emission–line stars can be used to estimate their evolutionary state, under certain assumptions. Cotera et al. (1996) asserted that the stars should be considered as WN type based on their spectral morphology and large measured line (velocity) widths. An alternate possibility (mentioned by Cotera et al. (1996) and Conti et al. (1995)) is that one or more of the Arches emission–line stars is a type Of supergiant. Conti et al. (1995) presented spectra of two O4 If supergiants which have similar spectral morphology as the late type WNs. These two objects appear to be similar in other respects to the late type WN stars (WNL) including the fact that they show particularly broad emission compared to other O If types (Leep 1979) and may be closely related in evolutionary status (Conti et al. 1995). It might be useful to remeasure the line widths at higher spectral resolution. Nebular contamination on small spatial scales and with differential velocity could cause the lines to appear more broad. This has recently been shown to be the case in the GC central cluster for a number of the He I stars (Paumard et al. 2001).

The similarity in spectral morphology for the Arches emission–line stars argues for a narrow range in evolutionary state independent of the type or class which they are compared to. However, taking the Cotera et al. (1996) conclusion that the Arches stars are WN type, then the ratio of $W_\lambda(2.19)$ to $W_\lambda(2.17)$ can be used to produce WN sub–types from the tabulated values for the optically classified WN stars presented by Figer et al. (1997). Table 5 gives the W_λ of each star with emission in both lines. From the ratio of these values, it is clear that the Arches stars occupy a narrow range centered on the sub–type WN7. Only one object (21) might have a low enough ratio to overlap with later WN8 stars; similarly, only one object (19) has an W_λ ratio between the values of the WN6 and WN7 objects in the Figer et al. (1997) catalog.

Some stars of WC sub–type have similar $W_\lambda(2.19)/W_\lambda(2.17)$ ratios to those for the Arches stars (Figer et al. 1997). However these WCs also typically have either He I 2.06 μm emission or show strong emission in the C IV triplet near 2.08 μm , which should be detected in the relatively broad red wing of the 2.06 μm filter (§2). The spectroscopic survey of Cotera et al. (1996) also

showed no evidence of C IV 2.08 μm or He I 2.06 μm emission in the bright Arches emission–line stars. Thus, stars of WC sub–type can be excluded from the presently identified emission–line star sample (but see also below).

The approximate spectral types allow us to estimate the age of the cluster. From evolutionary models at solar metallicity an age range between ~ 2.2 and 5.6 Myr is obtained for WNL stars by Maeder & Meynet (1994) for the standard mass loss rates. Solar Fe abundances have been measured for late–type supergiants (Carr et al. 2000; Ramírez et al. 2000) in the GC and nearby Quintuplet clusters, though the possibility still exists that the GC stellar population is metal rich in terms of alpha elements. Adopting the high mass loss models and/or models at twice solar metallicity gives a wider range of ~ 2 to 8 Myr. There are good indications that WN7 stars are descendants of stars with initial masses above $\sim 50 - 60 M_{\odot}$ (e.g. Schild & Maeder (1984), Crowther et al. (1995)). In this case, an upper age limit of $\lesssim 4-4.5$ Myr is obtained, independently of the exact metallicity and mass loss scenario.

A similar age is also deduced if the observed emission–line stars were O4 If stars (cf. above) or of the WN7 +abs type, which Crowther et al. (1995) have modeled and found intermediate between the Of and WNL stars. Blum et al. (1999) found a WN7+abs star at the heart of the young stellar cluster buried in the Galactic giant H II region W43. de Koter et al. (1997) concluded that two massive stars with Ofpe/WN6 or related WN types earlier than WN7 in the core of the R136 cluster in the LMC were infact main–sequence objects with a maximum age of 2 Myr; Massey & Hunter (1998) and Crowther & Dessart (1998) reached the same conclusion. Similar type stars are present in the dense core of NGC3603 (Drissen et al. 1995; Schmutz & Drissen 1999). In R136 and NGC3603, the stars are likely in a younger phase of evolution than the WN7 types (Crowther & Dessart 1998). The implication is thus that the Arches (and perhaps W43) is slightly more evolved than R136 and NGC3603; a point that will be checked in our subsequent paper when these data are used to estimate H abundances in the Arches emission–line stars. Figer et al. (1999) have suggested that the Arches may be $\approx 2 \pm 1$ Myr old based on near infrared photometry (consistent with the estimates discussed here), however near infrared colors and magnitudes are insensitive to age since even the evolved stars are on the Rayleigh–Jeans tail and so have very small color differences.

The age range of $\sim 2 - 4.5$ Myr is also compatible with the apparent absence of early type WN (WNE) and WC stars (which would indicate older ages; cf. Schild & Maeder (1984), Crowther et al. (1995)). However, WNE and WC stars are less luminous than WNL stars, and so it is possible that fainter emission–line stars have been missed. The WC stars are the faintest (Maeder & Meynet 1994). Blum et al. (1995*b*) have estimated the K –band magnitudes of the WC stars to be about 12.5 mag at a distance of 8 kpc, and extinction $A_K = 3$ mag, both appropriate for the Arches. Detections of the intrinsically less luminous stars will depend not only on the photometric completeness in each emission–line index filter (three per line), but also on the intrinsic line strengths which can be weak (Figer et al. 1997). The present observations are similar in angular resolution and field coverage as for the broad–band images presented by Figer et al. (1999), thus star counts for the brighter stars which are incomplete due to crowding should also be similar between the two

data sets. Figer et al. (1999) find that for stars with $K \lesssim 13.5$ the counts are $\gtrsim 50\%$ complete. Thus, if more than a few WNE or WC type stars with strong He II $2.19 \mu\text{m}$ or He I $2.06 \mu\text{m} + \text{C IV } \mu\text{m}$ emission were present in the cluster, a detection in either or both of Figures 2 and 4 would be expected (and depending on the object, in Figure 3, $\text{Br}\gamma$ as well), though we can not rule out the existence of weak-lined, older stars. For example, there is an object in Figure 2 at 11.5 mag with He II emission above the background. This is object no. 445 in our internal lists, and it has $W_\lambda = 21 \pm 7 \text{ \AA}$. This object is detected at $\text{Br}\gamma$ $2.17 \mu\text{m}$ but with only $1.4 \pm 4 \text{ \AA} W_\lambda$. The weaker lined WNE stars presented by Figer et al. (1997), WR 116 (WN6) and WR 133 (WN4.5 + O9.5 Ib), have similar He II emission, but stronger $\text{Br}\gamma$ emission.

In summary, the lack of strong lined WNE or WC detections suggests the bulk of the cluster is represented by the age (and large number) of the identified WNL stars, but the possibility of an older component can not be ruled out. A detailed analysis of the properties of the emission-line stars and comparisons with stellar models will be presented in a forthcoming paper.

4. Summary

Adaptive optics and HST/NICMOS images of high angular resolution have been presented in the emission-lines of He II $2.19 \mu\text{m}$, $\text{Br}\gamma$, He I $2.06 \mu\text{m}$, and $\text{P}\alpha$. Narrow-band indices and line fluxes have been computed for 300 to 500 stars in each line. The line calculations will be used in a following paper to derive detailed models for the subset of massive stars first identified by Nagata et al. (1995) and Cotera et al. (1996). The tight sequences indicated in narrow-band indices demonstrate that adaptive optics observations can be used to determine accurate fluxes, even in crowded regions.

Comparison of the data presented here to previous line fluxes shows generally good agreement in the $\text{Br}\gamma$ line, especially for the objects farthest from the crowded core of the Arches cluster. Evidence was presented for one object which suggests its combination of line fluxes suggests it may have varied intrinsically between these observations and previous ones. Other objects show larger differences, chiefly in the nebular $\text{Br}\gamma$ line and in the more central region of the cluster. It is suggested that these differences may be due the difference in angular resolution between the present and past data sets.

Two new emission-line stars have been identified. One is a bright object which was $\sim 10''$ south of the region previously surveyed. The other is somewhat fainter but in the more crowded region of the central cluster, so that it was not apparent in earlier lower angular resolution work. The narrow-band fluxes presented here suggest these objects are similar in nature to the other massive stars already identified in the Arches. In addition three additional candidate stars in the cluster were identified. These are fainter objects with somewhat weaker lines detected at lower significance. Significant differences in the spectroscopic character of Cotera star 11 indicate that real changes may have occurred between the earlier observations (1992/1993) of Cotera et al. (1996)

and those presented here.

Detailed spectral types are presented for the Arches emission–line stars with 2.19 μm and 2.17 μm emission under the assumption that they are Wolf–Rayet stars. Irrespective of the precise spectral type, the emission–line character of the bright cluster stars is remarkably similar, hence the evolutionary spread is quite narrow. From the approximate spectral types of the identified emission–line stars and comparisons with evolutionary models we infer a cluster age between ~ 2 and 4.5 Myr.

The authors would like to thank the staff of the CFHT for their excellent support while at the telescope and François Ménard for assistance with filter transmission curves. The authors also acknowledge D. Figer for taking the original $P\alpha$ data as part of his HST/NICMOS Arches program. Finally, the authors thank A. Cotera for useful discussions about the calibration of the HST images.

REFERENCES

- Allen, D. A., Hyland, A. R., Hillier, D. J. 1990, MNRAS, 244, 706
- Beuzit, J. L. & Hainaut, M. C. 1998, Users Manual for the CFHT Adaptive Optics Bonnette PUEO and its associated cameras KIR and FOCAM, CFHT, Version 0.9
- Blum, R. D., DePoy, D. L., & Sellgren, K. 1995, ApJ, 441, 603
- Blum, R. D., Sellgren, K., & Depoy, D. L. 1995, ApJ, 440, L17
- Blum, R. D. & Daminieli, A. 1999, ApJ, 512, 237
- Blum, R.D., Daminieli, A., & Conti, P.S. 1999, AJ, 117, 1392
- Carr, J. S., Sellgren, K., & Balachandran, S. C. 2000, ApJ, 530, 307
- Conti, P. S., Hanson, M. M., Morris, P. W., Willis, A. J., & Fossey, S. J. 1995, ApJ, 445, L35
- Cotera, A. S., Erickson, E. F., Colgan, S. W. J., Simpson, J. P., Allen, D. A., & Burton, M. G. 1996, ApJ, 461, 750
- Crowther, P. A., Smith, L. J., Hillier, D. J., & Schmutz, W. 1995, A&A, 293, 427
- Crowther, P. A. & Smith, L. J. 1996, A&A, 305, 541
- Crowther, P. A. & Dessart, L. 1998, MNRAS, 296, 622
- Drissen, L., Moffat, A. F. J., Walborn, N. R., & Shara, M. M. 1995, AJ, 110, 2235
- Elias, J. H., Frogel, J. A., Matthews, K., & Neugebauer, G. 1982, AJ, 87, 1029
- Figer, D. F., McLean, I. S., & Najarro, F. 1997, ApJ, 486, 420

- Figer, D. F., Kim, S. S., Morris, M., Serabyn, E., Rich, R. M., & McLean, I. S. 1999, *ApJ*, 525, 750
- Forrest, W. J., Shure, M. A., Pipher, J. L., & Woodward, C. E. 1987, *AIP Conf. Proc.* 155: The Galactic Center, 153
- Hanson, M. M., Conti, P. S., & Rieke, M. J. 1996, *ApJS*, 107 281
- Holtzman, J. 2001, <http://ganymede.nmsu.edu/holtz/xvista/index.html>
- van der Hucht, K. A. 2001, *New Astronomy Review*, 45, 135
- Johnson, H. 1966, *ARA&A*, 4, 193
- de Koter, A., Heap, S. R., & Hubeny, I. 1997, *ApJ*, 477, 792
- Krabbe, A., Genzel, R., Drapatz, S., & Rotaciuc, V. 1991, *ApJ*, 382, L19
- Leep, E. M. 1979, *IAU Symp.* 83: Mass Loss and Evolution of O-Type Stars, 83, 471
- Maeder, A. & Meynet, G. 1994, *A&A*, 287, 803
- Massey, P. & Hunter, D. A. 1998, *ApJ*, 493, 180
- Mathis, J.S. 1990, *ARA&A*, 28, 37
- Morris, M. & Yusef-Zadeh, F. 1985, *AJ*, 90, 2511
- Morris, M. & Serabyn, E. 1996, *ARA&A*, 34, 645
- Nagata, T., Woodward, C. E., Shure, M., & Kobayashi, N. 1995, *AJ*, 109, 1676
- Paumard, T., Maillard, J. P., Morris, M., & Rigaut, F. 2001, *A&A*, 366, 466
- Ramírez, S. V., Sellgren, K., Carr, J. S., Balachandran, S. C., Blum, R., Terndrup, D. M., & Steed, A. 2000, *ApJ*, 537, 205
- Rieke, M. 2001, private communication
- Rigaut, F. et al. 1998, *PASP*, 110, 152
- Salpeter, E. E. 1955, *ApJ*, 121, 161
- Schild, H., Maeder, A., 1984, *A&A*, 136, 237
- Schmutz W. & Drissen L. 1999, *Rev. Mex. A&A Ser. Conf.* 8, 41–48
- Serabyn, E., Shupe, D., & Figer, D. F. 1998, *Nature*, 394, 448
- Stetson, P. 1987, *PASP*, 99, 191

Tokunaga, A. T. 1986, NASA IRTF Photometry Manual, p. 16

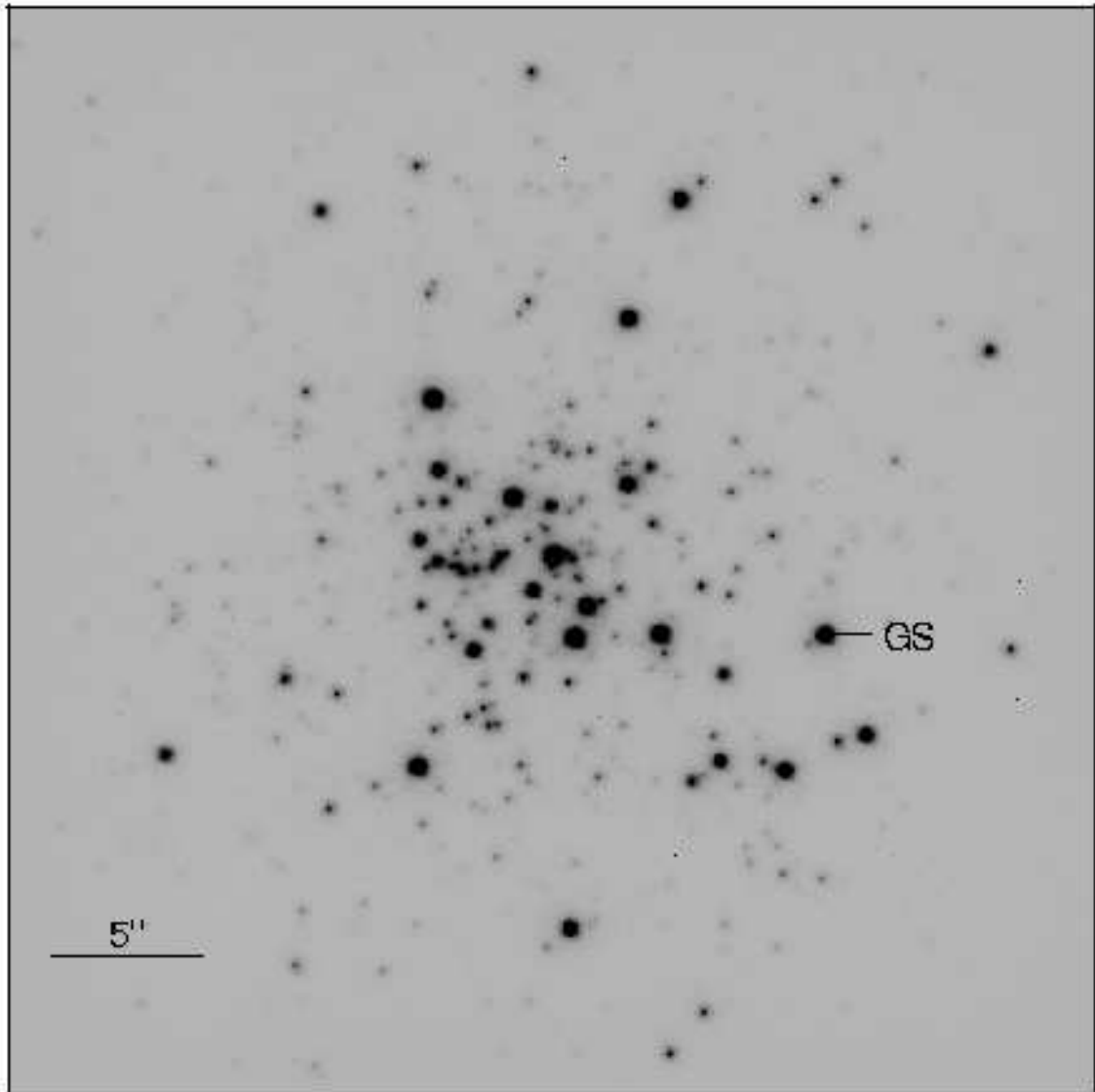


Fig. 1a.— He II $2.19 \mu\text{m}$ CFHT adaptive optics bonnette image of the Arches cluster. North is up, East to the left, and the scale is $0.035'' \text{ pix}^{-1}$ in this $\sim 36'' \times 36''$ image. The adaptive optics guide star is labeled “GS.”

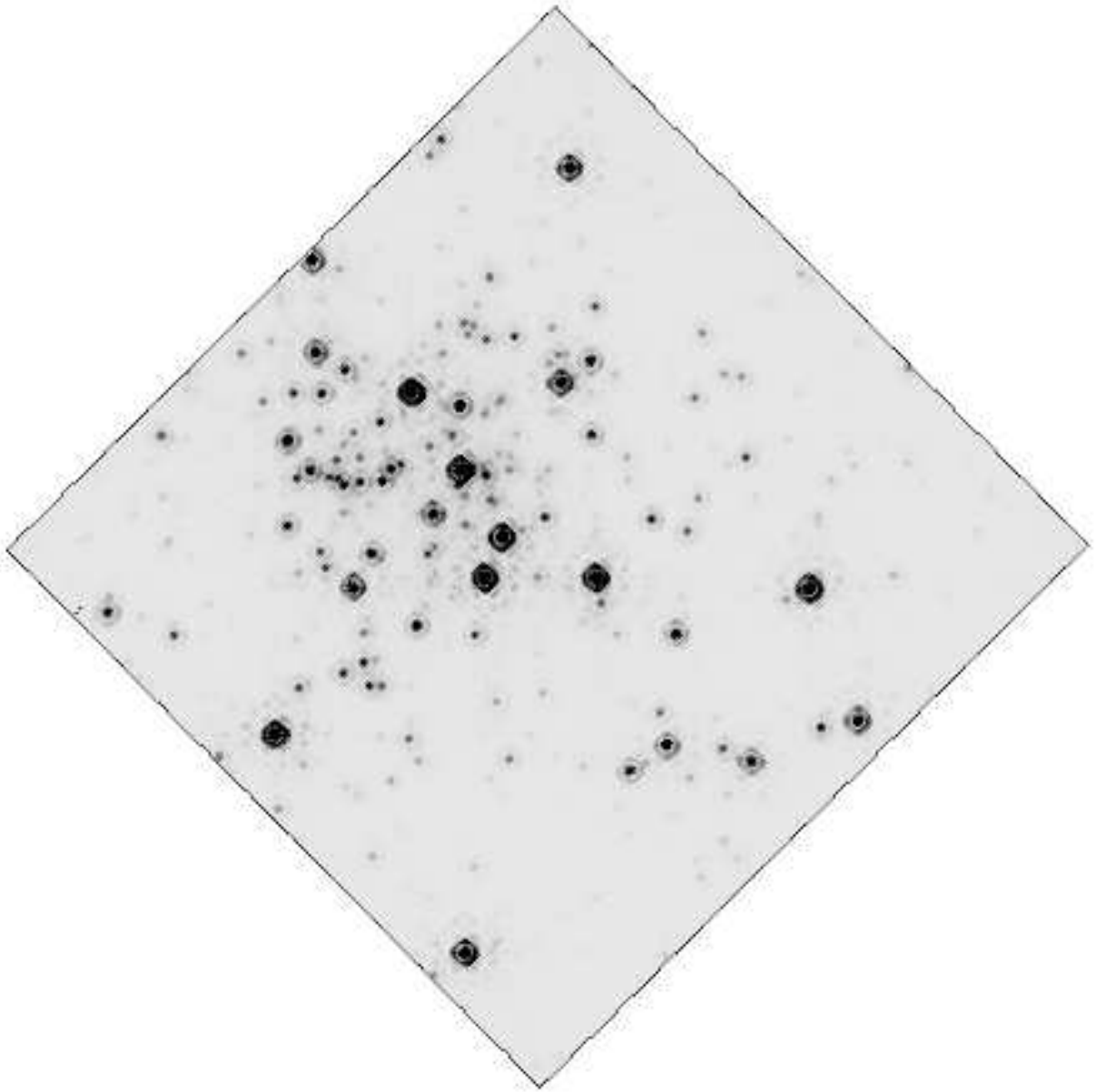


Fig. 1*b*.— F187 ($P\alpha$) HST/NICMOS image. North up and East to the left. This image has been rotated by -44.7 degrees counter-clockwise from the original orientation. The scale is $0.076'' \text{ pix}^{-1}$ in this $19'' \times 19''$ image.

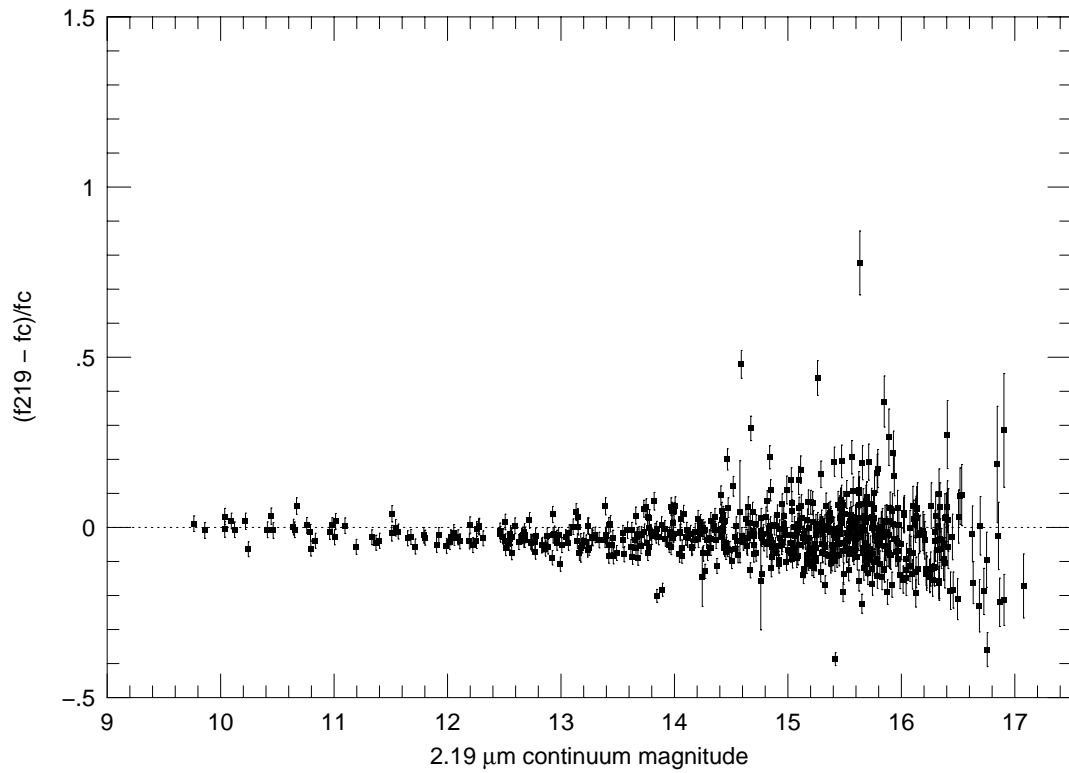


Fig. 2.— He II 2.19 μm Narrow-band index. The index is similar to an equivalent width; see text. Line fluxes and equivalent widths in Tables 4 and 5 have been corrected for the systematic “absorption” evident in this plot; see text.

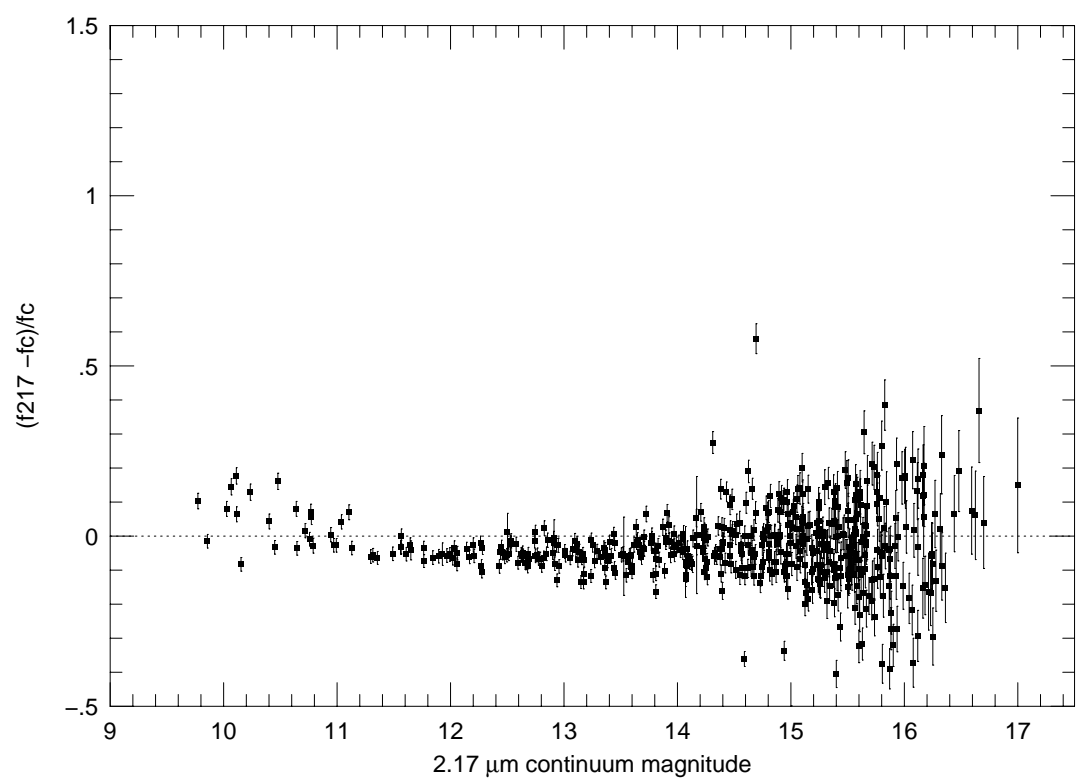


Fig. 3.— Same as Figure 2 but for the Br γ line.

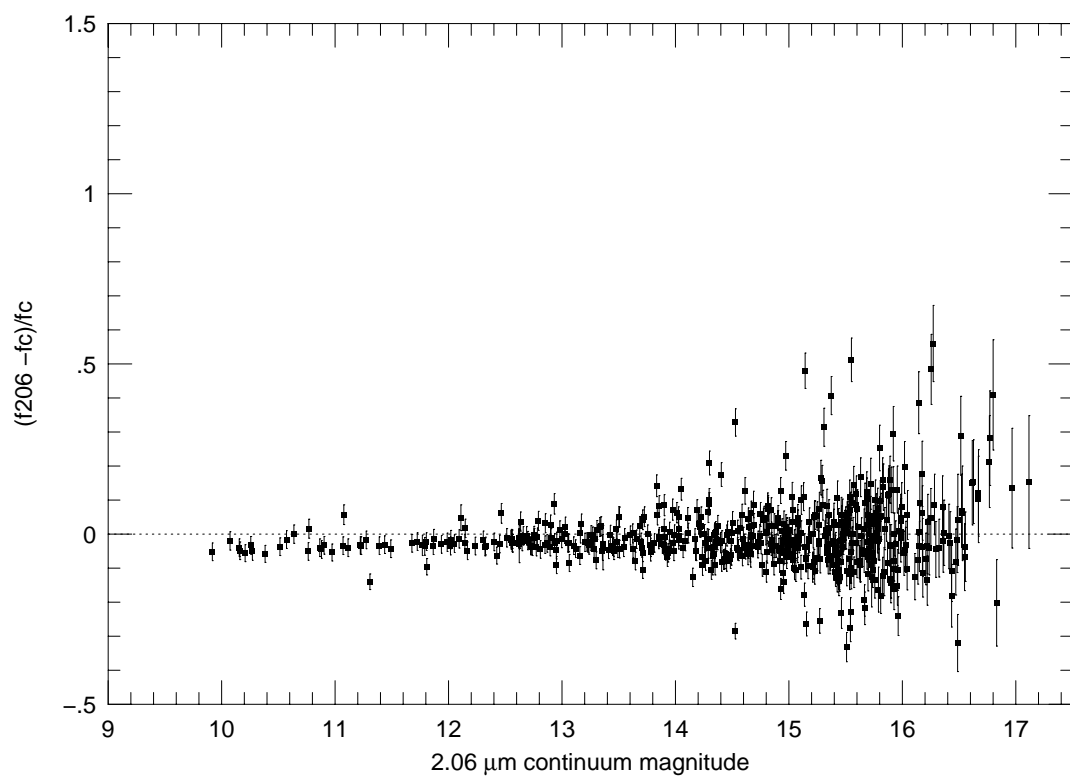


Fig. 4.— Same as Figure 2 but for the He I 2.06 μm line.

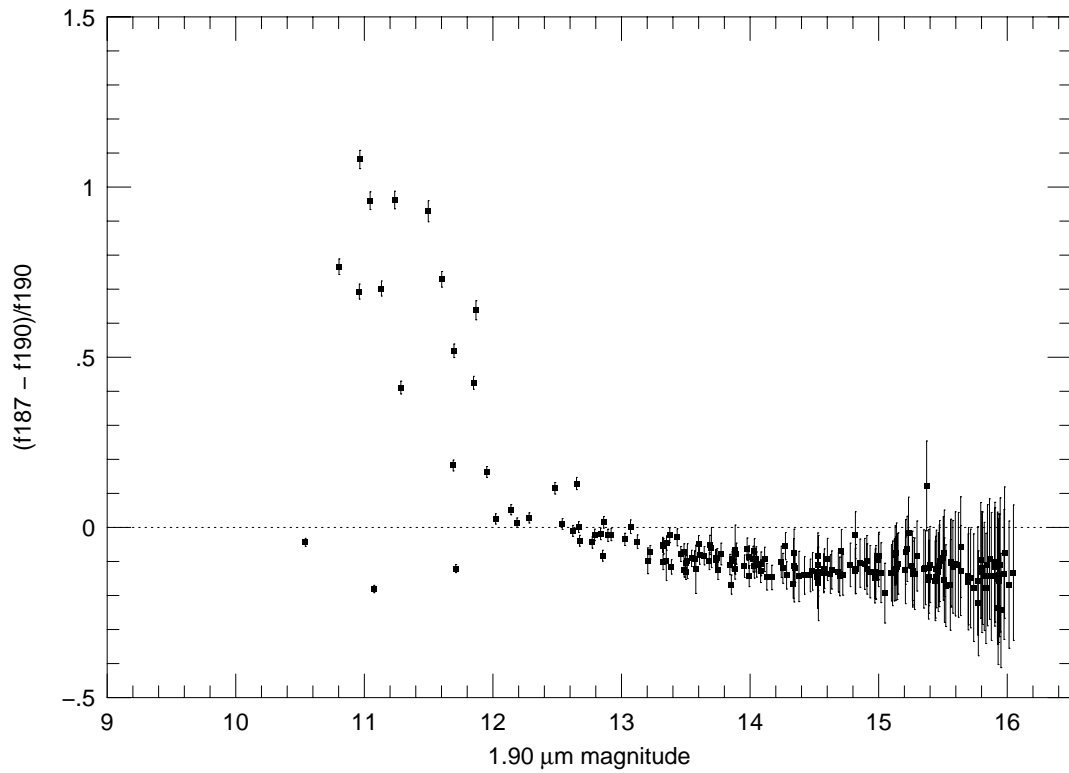


Fig. 5.— Same as Figure 2 but for the $P\alpha$ line. This index differs from the $2\ \mu\text{m}$ indices because it has no blue continuum point; see text. The line fluxes and equivalent widths for $P\alpha$ are not corrected for the systematic “absorption” evident in this plot; see text.

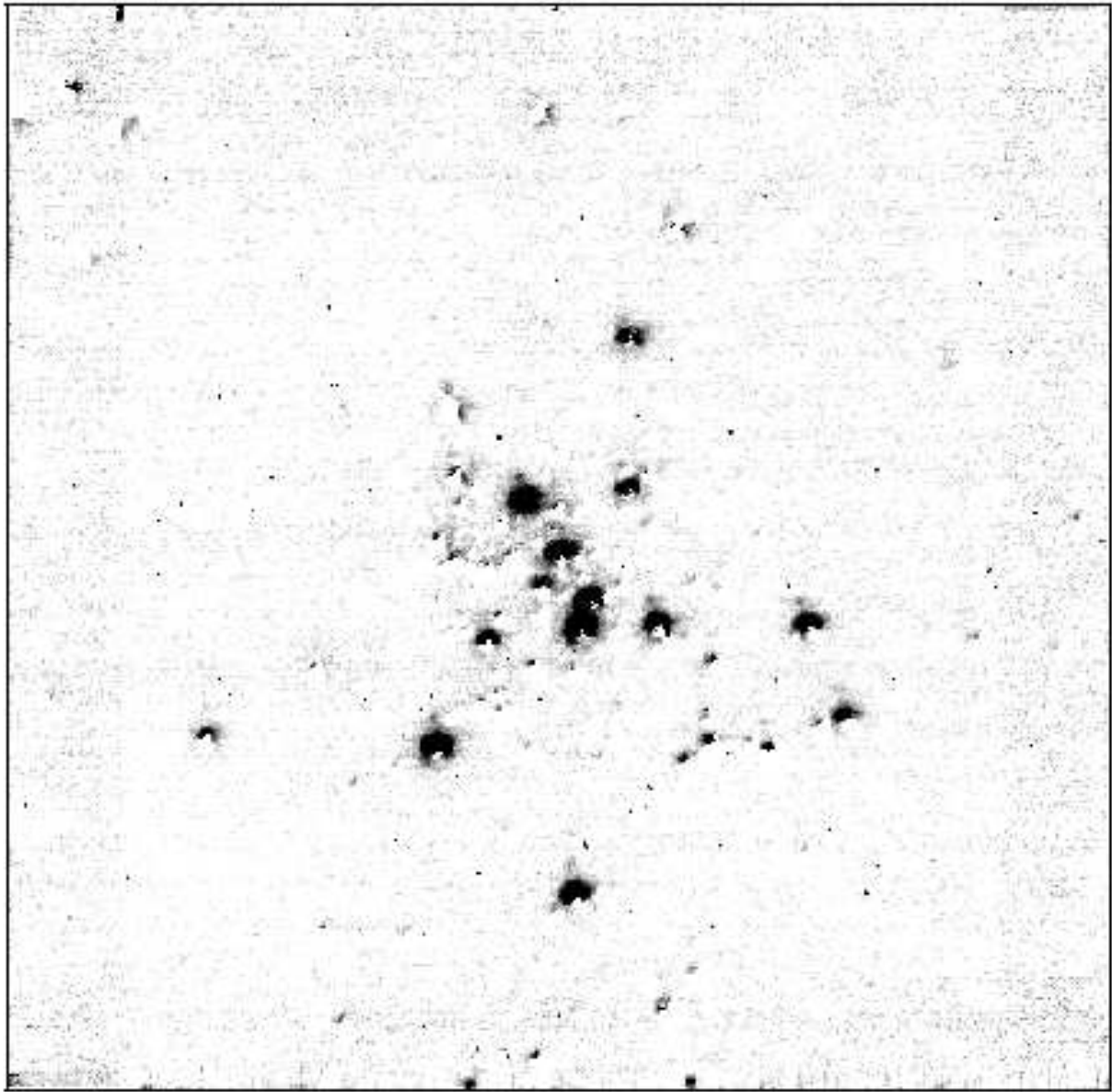


Fig. 6.— $\text{Br}\gamma$. Continuum subtracted $2.17 \mu\text{m}$ image using the $2.26 \mu\text{m}$ continuum (for simplicity). The adaptive optics guide star appears as a false emission-line star due to its strong blue continuum, but the detailed photometry using two continuum points accounts for this; see text. The bright object to the south of the image is a newly identified emission-line star.

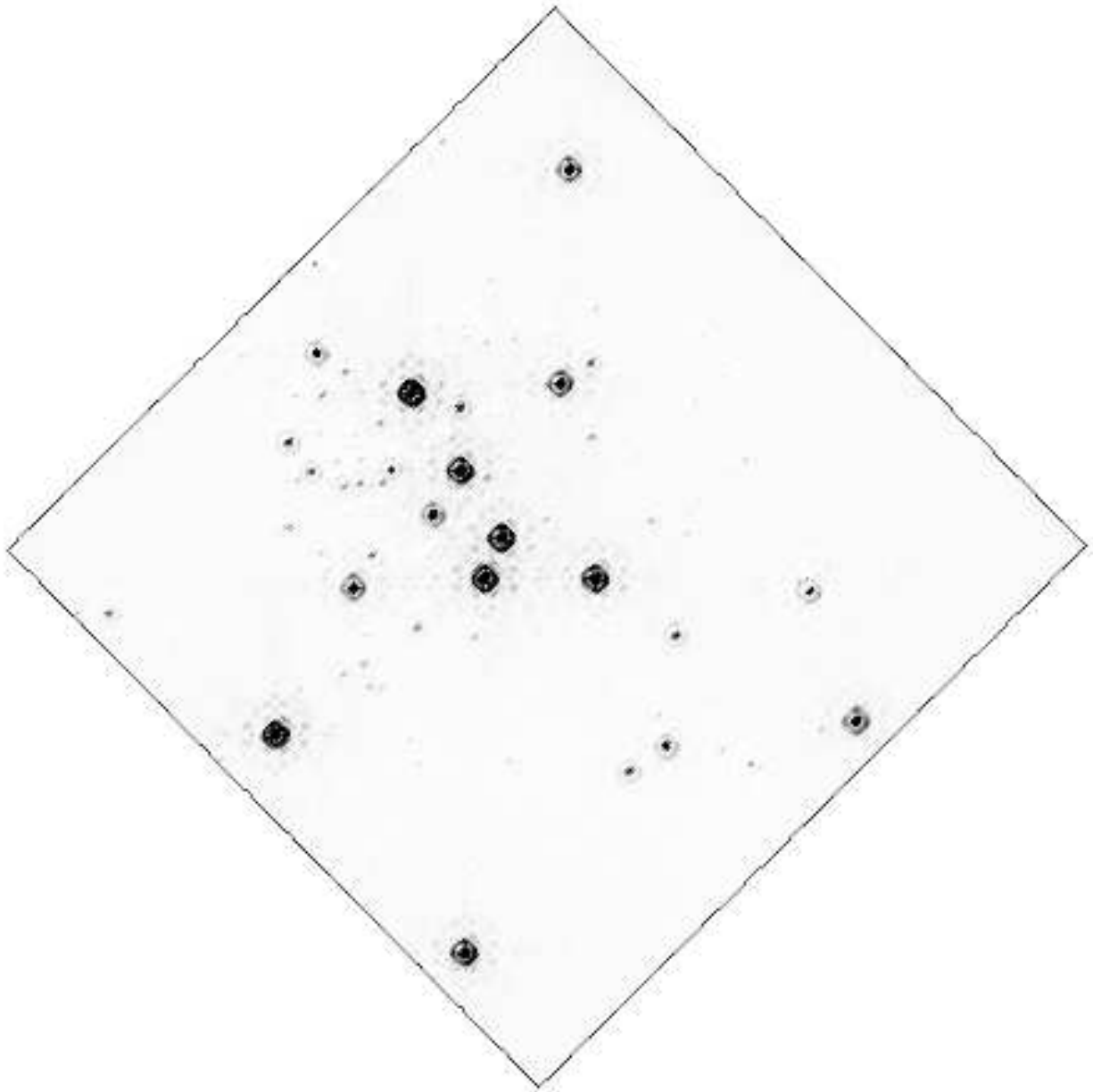


Fig. 7.— $P\alpha$ $1.87\ \mu\text{m}$ continuum subtracted image. The bright object near the bottom is a newly identified emission-line star.

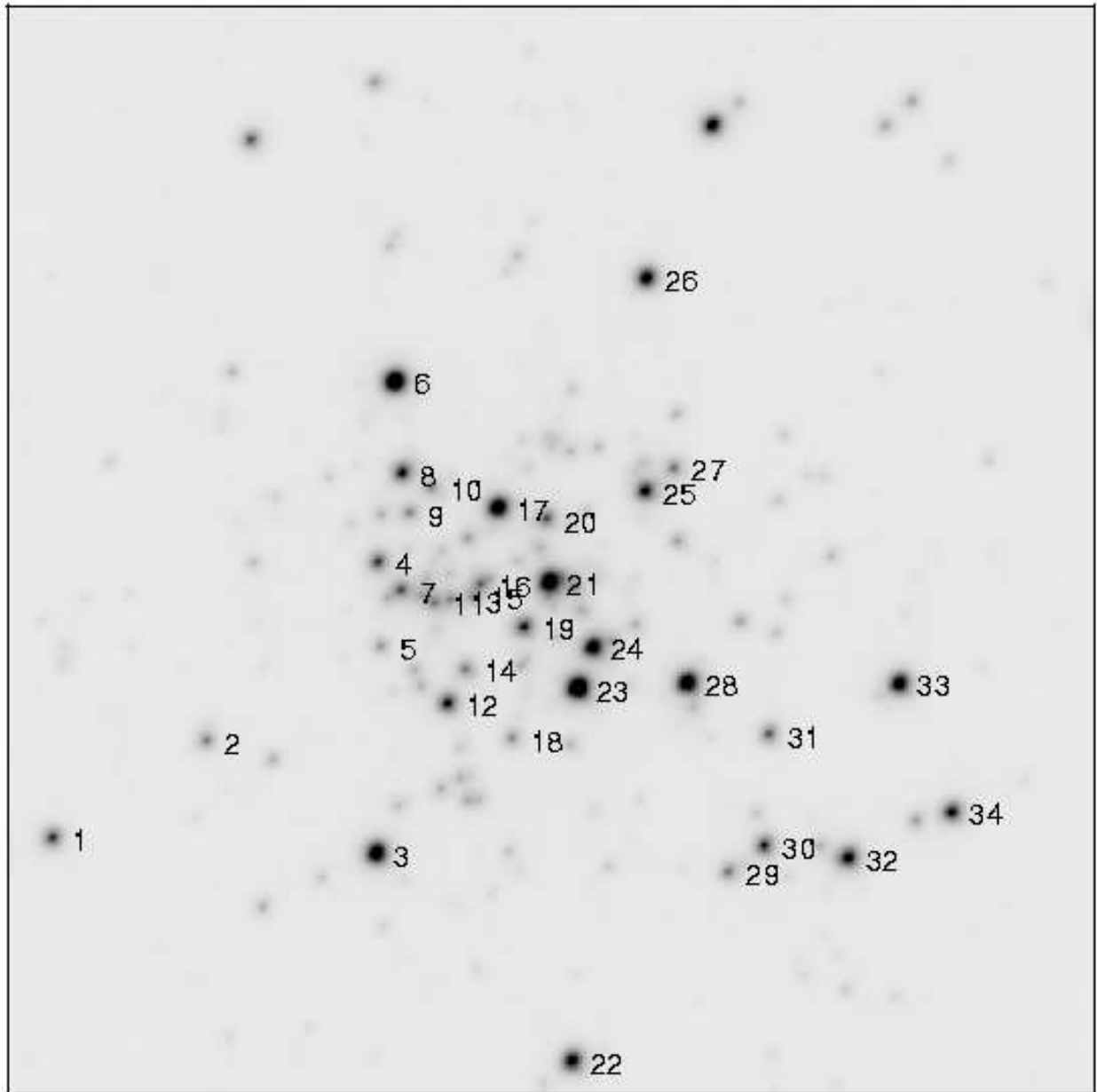


Fig. 8.— Positions of stars corresponding to the IDs in Tables 2, 3, and 4 overlaid on the $2.26\ \mu\text{m}$ image. The region shown is smaller ($28'' \times 28''$) than in Figure 1a, but the orientation is the same. Corresponding IDs for Nagata et al. (1995) and Cotera et al. (1996) are given in Table 4.

Table 1. Wolf-Rayet Star Observed Line Strengths (\AA)

Star	Sp Type	He I 2.06 μm	Lit ^b	Δ^c	Br γ 2.17 μm	Lit ^b	Δ^c	He II 2.19 μm	Lit ^b	Δ	He II/Br γ
WR122	Ofpe/WN9	623 ^a	680	-0.08	25	22	0.14	
WR123	WN8	48 ^a	77	-0.38	65	74	-0.12	26	19	0.37	0.40
WR128	WN4	43	44	-0.02	63	76	-0.17	1.47
WR131	WN7+abs	47	41	0.15	220	18	... ^d	4.68
WR134	WN6	75	83	-0.10	129	137	-0.06	1.72
WR138	WN5+O9	49	35	0.40	65	54	0.20	1.33
mean						0.07			0.09		
stddev						0.08			0.12		

^aContinuum is based on 2.14 μm point only; see text

^bValues for equivalent widths from spectroscopic measurements are from Blum et al. (1995a), Crowther & Smith (1996), and Figer et al. (1997).

^cDifference in equivalent width as a percentage of the literature value

^dThe narrow-band He II line for WR131 is an order of magnitude stronger than the literature value (Figer et al. 1997); see discussion in §2.1.3

Table 2. Arches Emission-Line Star Positions

Star ID	RA ($''$) ^a	DEC ($''$) ^a	Radius ($''$) ^a
1	21.8	-4.0	22.2
2	17.9	-1.5	17.9
3	13.5	-4.4	14.2
4	13.4	3.1	13.8
5	13.4	1.0	13.4
6	13.0	7.8	15.1
7	12.8	2.4	13.1
8	12.8	5.4	13.9
9	12.6	4.4	13.4
10	12.1	5.0	13.1
11	12.0	2.1	12.2
12	11.6	-0.5	11.6
13	11.6	2.2	11.8
14	11.2	0.4	11.2
15	11.0	2.2	11.2
16	10.8	2.6	11.1
17	10.3	4.5	11.3
18	10.0	-1.4	10.1
19	9.7	1.5	9.8
20	9.1	4.3	10.0
21	9.0	2.6	9.4
22	8.4	-9.7	12.9
23	8.3	-0.1	8.3
24	7.9	0.9	8.0
25	6.5	5.0	8.2
26	6.5	10.5	12.3
27	5.8	5.6	8.0
28	5.5	0.0	5.5
29	4.4	-4.9	6.6
30	3.5	-4.2	5.4
31	3.4	-1.3	3.6
32	1.3	-4.5	4.7
33	0.0	0.0	0.0

Table 2—Continued

Star ID	RA (") ^a	DEC (") ^a	Radius (") ^a
34	-1.4	-3.3	3.6

^aOffset from the adaptive optics guide star, Star ID 33; see also Figure 1*a*.

Table 3. Arches Emission-Line Star Narrow-band Magnitudes

Star ID	2.26 μm	2.19 μm	2.17 μm	2.14 μm	2.06 μm	2.03 μm	1.90 μm	1.87 μm
1	11.08 \pm 0.01	11.10 \pm 0.02	11.03 \pm 0.01	11.11 \pm 0.03	11.29 \pm 0.03	11.34 \pm 0.02	...	nodata
2	11.78 \pm 0.01	11.79 \pm 0.02	11.80 \pm 0.01	11.76 \pm 0.03	11.88 \pm 0.03	11.91 \pm 0.02	12.67 \pm 0.01	12.69 \pm 0.01
3	10.13 \pm 0.01	10.09 \pm 0.02	9.94 \pm 0.01	10.10 \pm 0.03	10.29 \pm 0.03	10.32 \pm 0.02	11.05 \pm 0.01	10.34 \pm 0.01
4	11.15 \pm 0.01	11.19 \pm 0.02	11.17 \pm 0.01	11.12 \pm 0.03	11.27 \pm 0.03	11.27 \pm 0.02	12.02 \pm 0.01	12.02 \pm 0.01
5	12.10 \pm 0.01	12.11 \pm 0.02	12.11 \pm 0.01	12.05 \pm 0.03	12.22 \pm 0.03	12.21 \pm 0.02	12.92 \pm 0.01	12.97 \pm 0.01
6	9.80 \pm 0.01	9.86 \pm 0.02	9.87 \pm 0.01	9.88 \pm 0.03	10.20 \pm 0.03	10.28 \pm 0.02	11.07 \pm 0.01	11.31 \pm 0.01
7	11.35 \pm 0.01	11.37 \pm 0.02	11.38 \pm 0.01	11.31 \pm 0.03	11.47 \pm 0.03	11.49 \pm 0.02	12.19 \pm 0.01	12.19 \pm 0.01
8	10.82 \pm 0.01	10.84 \pm 0.02	10.82 \pm 0.02	10.78 \pm 0.03	10.93 \pm 0.03	10.92 \pm 0.02	11.69 \pm 0.01	11.53 \pm 0.01
9	11.87 \pm 0.01	11.90 \pm 0.02	11.91 \pm 0.01	11.83 \pm 0.03	11.97 \pm 0.03	11.98 \pm 0.02	12.67 \pm 0.01	12.74 \pm 0.01
10	11.94 \pm 0.02	11.99 \pm 0.02	11.99 \pm 0.03	11.92 \pm 0.03	12.04 \pm 0.03	12.06 \pm 0.02	12.79 \pm 0.01	12.84 \pm 0.01
11	12.00 \pm 0.01	12.02 \pm 0.02	12.03 \pm 0.01	11.96 \pm 0.03	12.08 \pm 0.03	12.09 \pm 0.02	12.84 \pm 0.01	12.88 \pm 0.01
12	10.80 \pm 0.01	10.79 \pm 0.02	10.71 \pm 0.01	10.76 \pm 0.03	10.94 \pm 0.03	10.96 \pm 0.02	11.70 \pm 0.01	11.27 \pm 0.01
13	12.02 \pm 0.01	12.03 \pm 0.02	12.05 \pm 0.01	11.98 \pm 0.03	12.11 \pm 0.03	12.14 \pm 0.02	12.86 \pm 0.01	12.87 \pm 0.01
14	11.80 \pm 0.01	11.80 \pm 0.02	11.85 \pm 0.01	11.75 \pm 0.03	11.90 \pm 0.03	11.91 \pm 0.02	12.62 \pm 0.01	12.65 \pm 0.01
15	12.09 \pm 0.01	12.09 \pm 0.02	12.15 \pm 0.01	12.05 \pm 0.03	12.17 \pm 0.03	12.18 \pm 0.02	12.89 \pm 0.01	12.94 \pm 0.01
16	11.64 \pm 0.01	11.65 \pm 0.02	11.67 \pm 0.01	11.60 \pm 0.03	11.75 \pm 0.03	11.77 \pm 0.02	12.48 \pm 0.01	12.39 \pm 0.01
17	10.10 \pm 0.01	10.04 \pm 0.02	9.92 \pm 0.01	10.06 \pm 0.03	10.27 \pm 0.03	10.27 \pm 0.02	10.97 \pm 0.01	10.19 \pm 0.01
18	11.92 \pm 0.01	11.92 \pm 0.02	11.96 \pm 0.01	11.89 \pm 0.03	12.06 \pm 0.03	12.07 \pm 0.02	12.77 \pm 0.01	12.84 \pm 0.01
19	10.98 \pm 0.01	10.96 \pm 0.02	10.94 \pm 0.01	10.93 \pm 0.03	11.11 \pm 0.03	11.13 \pm 0.02	11.85 \pm 0.01	11.49 \pm 0.01
20	11.34 \pm 0.01	11.33 \pm 0.02	11.36 \pm 0.01	11.28 \pm 0.03	11.43 \pm 0.03	11.43 \pm 0.02	12.14 \pm 0.01	12.11 \pm 0.01
21	10.05 \pm 0.01	10.04 \pm 0.02	9.94 \pm 0.01	10.02 \pm 0.03	10.22 \pm 0.03	10.22 \pm 0.02	10.96 \pm 0.01	10.41 \pm 0.01
22	10.50 \pm 0.01	10.44 \pm 0.02	10.32 \pm 0.01	10.47 \pm 0.03	10.64 \pm 0.03	10.71 \pm 0.02	11.50 \pm 0.01	10.81 \pm 0.01
23	9.80 \pm 0.01	9.76 \pm 0.02	9.67 \pm 0.01	9.76 \pm 0.03	9.98 \pm 0.03	9.98 \pm 0.02	10.80 \pm 0.01	10.21 \pm 0.01
24	10.26 \pm 0.01	10.22 \pm 0.02	10.10 \pm 0.01	10.23 \pm 0.03	10.45 \pm 0.03	10.45 \pm 0.02	11.24 \pm 0.01	10.53 \pm 0.01
25	10.66 \pm 0.01	10.64 \pm 0.02	10.56 \pm 0.01	10.63 \pm 0.03	10.82 \pm 0.03	10.82 \pm 0.02	11.60 \pm 0.01	11.03 \pm 0.01

Table 3—Continued

Star ID	2.26 μm	2.19 μm	2.17 μm	2.14 μm	2.06 μm	2.03 μm	1.90 μm	1.87 μm
26	10.43 \pm 0.01	10.41 \pm 0.02	10.36 \pm 0.01	10.39 \pm 0.03	10.55 \pm 0.03	10.56 \pm 0.02	11.28 \pm 0.01	10.93 \pm 0.01
27	11.68 \pm 0.01	11.72 \pm 0.02	11.70 \pm 0.03	11.64 \pm 0.03	11.81 \pm 0.03	11.82 \pm 0.03	12.54 \pm 0.01	12.55 \pm 0.01
28	10.13 \pm 0.01	10.12 \pm 0.02	10.05 \pm 0.01	10.11 \pm 0.03	10.33 \pm 0.03	10.34 \pm 0.02	11.13 \pm 0.01	10.58 \pm 0.01
29	11.66 \pm 0.01	11.68 \pm 0.02	11.67 \pm 0.01	11.64 \pm 0.03	11.83 \pm 0.03	11.85 \pm 0.02	12.65 \pm 0.01	12.54 \pm 0.01
30	10.98 \pm 0.01	11.00 \pm 0.02	11.00 \pm 0.01	10.97 \pm 0.03	11.16 \pm 0.03	11.18 \pm 0.02	11.95 \pm 0.01	11.81 \pm 0.01
31	11.37 \pm 0.01	11.40 \pm 0.02	11.43 \pm 0.01	11.35 \pm 0.03	11.54 \pm 0.03	11.55 \pm 0.02	12.28 \pm 0.01	12.27 \pm 0.01
32	10.63 \pm 0.01	10.65 \pm 0.02	10.69 \pm 0.01	10.65 \pm 0.03	10.91 \pm 0.03	10.96 \pm 0.02	11.71 \pm 0.01	11.87 \pm 0.01
33	10.35 \pm 0.01	10.24 \pm 0.02	10.25 \pm 0.01	10.10 \pm 0.03	10.10 \pm 0.03	10.07 \pm 0.02	10.54 \pm 0.01	10.61 \pm 0.01
34	10.74 \pm 0.01	10.76 \pm 0.02	10.69 \pm 0.01	10.78 \pm 0.03	11.03 \pm 0.03	11.06 \pm 0.02	11.87 \pm 0.02	11.35 \pm 0.01

Table 4. Arches Emission-Line Star Line Fluxes ($\text{W-cm}^{-2} \times 10^{21}$)

Star ID	Other ID ^a	He II 2.19 μm^{b}	Br γ ^b	He I 2.06 μm^{b}	P α
1	10	1.43 \pm 0.89	3.12 \pm 0.63	0.05 \pm 1.23	...
2		0.31 \pm 0.47	0.00 \pm 0.31	0.23 \pm 0.68	0.00 \pm 0.22
3	11, N14	5.69 \pm 2.25	15.51 \pm 1.72	-0.75 \pm 3.12	46.79 \pm 1.46
4	4	-1.12 \pm 0.82	0.00 \pm 0.55	-0.31 \pm 1.22	0.60 \pm 0.20
5		-0.12 \pm 0.35	-0.12 \pm 0.23	-0.43 \pm 0.52	-0.17 \pm 0.17
6	A, N13	3.17 \pm 2.78	2.67 \pm 1.84	-1.79 \pm 3.82	-8.61 \pm 0.48
7		-0.59 \pm 0.69	-0.47 \pm 0.46	-0.25 \pm 1.02	0.17 \pm 0.17
8	B, N12, Candidate	-0.38 \pm 1.13	0.38 \pm 0.76	-1.42 \pm 1.67	4.87 \pm 0.54
9		-0.36 \pm 0.42	-0.29 \pm 0.28	-0.16 \pm 0.63	-0.44 \pm 0.22
10		-0.33 \pm 0.39	-0.13 \pm 0.39	0.02 \pm 0.58	-0.20 \pm 0.20
11		-0.13 \pm 0.38	-0.26 \pm 0.25	-0.15 \pm 0.56	-0.19 \pm 0.19
12	7	1.34 \pm 1.18	3.85 \pm 0.85	-0.41 \pm 1.70	13.93 \pm 0.54
13		0.06 \pm 0.38	-0.12 \pm 0.25	0.18 \pm 0.55	0.09 \pm 0.18
14		0.08 \pm 0.47	-0.46 \pm 0.30	-0.17 \pm 0.68	-0.11 \pm 0.23
15		0.06 \pm 0.36	-0.47 \pm 0.22	-0.13 \pm 0.52	-0.18 \pm 0.18
16	Candidate	0.09 \pm 0.53	-0.18 \pm 0.35	0.03 \pm 0.78	1.57 \pm 0.26
17	2, N11	7.01 \pm 2.35	13.37 \pm 1.75	-3.57 \pm 3.23	56.67 \pm 1.57
18		0.27 \pm 0.42	-0.27 \pm 0.27	-0.32 \pm 0.60	-0.40 \pm 0.20
19	New	1.15 \pm 1.01	1.32 \pm 0.68	-0.35 \pm 1.45	10.03 \pm 0.47
20		0.12 \pm 0.72	-0.47 \pm 0.47	-0.26 \pm 1.05	0.89 \pm 0.18
21	5, N10	2.68 \pm 2.35	9.22 \pm 1.72	-2.74 \pm 3.36	36.54 \pm 1.06
22	New	4.85 \pm 1.63	10.10 \pm 1.21	1.33 \pm 2.22	29.95 \pm 0.97
23	8, N8	6.33 \pm 3.05	13.55 \pm 2.21	-3.41 \pm 4.26	47.25 \pm 1.23
24	6, N7	5.05 \pm 1.99	10.79 \pm 1.48	-3.02 \pm 2.77	39.28 \pm 1.23
25	3, N6	2.18 \pm 1.35	5.21 \pm 0.97	-1.57 \pm 1.91	21.44 \pm 0.59
26	1, N5	1.91 \pm 1.67	4.33 \pm 1.17	-1.30 \pm 2.39	16.17 \pm 0.79
27		-0.69 \pm 0.50	0.00 \pm 0.51	-0.19 \pm 0.75	0.12 \pm 0.25
28	9, N4	2.49 \pm 2.19	7.07 \pm 1.55	-2.47 \pm 3.09	31.70 \pm 0.91
29	Candidate	0.09 \pm 0.52	0.17 \pm 0.35	-0.40 \pm 0.75	1.45 \pm 0.22
30	12	0.16 \pm 0.97	0.32 \pm 0.65	-0.74 \pm 1.40	3.40 \pm 0.43
31	E	-0.23 \pm 0.67	-0.45 \pm 0.44	-0.52 \pm 0.99	0.47 \pm 0.16
32	G, N3	1.53 \pm 1.34	0.00 \pm 0.86	-0.93 \pm 1.88	-3.18 \pm 0.27
33	F, N2, GS ^c	-2.68 \pm 1.96	-2.69 \pm 1.29	0.15 \pm 3.12	-3.12 \pm 0.78

Table 4—Continued

Star ID	Other ID ^a	He II 2.19 μm ^b	Br γ ^b	He I 2.06 μm ^b	P α
34	13, N1	2.52 \pm 1.21	4.27 \pm 0.86	-1.30 \pm 1.67	14.66 \pm 0.69

^aEmission-line star ID from Cotera et al. (1996), Nagata et al. (1995) (“N”), or other ID from this paper.

^bFlux has been corrected for intrinsic absorption in O and B-type stars; see §3.1.

^cAdaptive optics guide star; see Figure 1*a*.

Table 5. Arches Emission-Line Star Line Equivalent Widths (\AA)

Star ID	He II 2.19 μm^a	Br γ ^a	He I 2.06 μm^a	P α^a	He II 2.19 $\mu\text{m}/\text{Br}\gamma$	SpTyp ^b
1	10.00 \pm 6.00	22.00 \pm 4.00	0.40 \pm 8.40	0.00 \pm 0.00	0.45	WN7
2	4.00 \pm 6.00	0.00 \pm 4.00	3.20 \pm 8.40	0.00 \pm 3.70
3	16.00 \pm 6.00	44.00 \pm 4.00	-2.40 \pm 8.40	179.50 \pm 5.60	0.36	WN7
4	-8.00 \pm 6.00	0.00 \pm 4.00	-2.40 \pm 8.40	5.60 \pm 1.90
5	-2.00 \pm 6.00	-2.00 \pm 4.00	-8.00 \pm 8.40	-3.70 \pm 3.70
6	7.00 \pm 6.00	6.00 \pm 4.00	-5.20 \pm 8.40	-33.70 \pm 1.90
7	-5.00 \pm 6.00	-4.00 \pm 4.00	-2.40 \pm 8.40	1.90 \pm 1.90
8	-2.00 \pm 6.00	2.00 \pm 4.00	-8.00 \pm 8.40	33.70 \pm 3.70
9	-5.00 \pm 6.00	-4.00 \pm 4.00	-2.40 \pm 8.40	-7.50 \pm 3.70
10	-5.00 \pm 6.00	-2.00 \pm 6.00	0.40 \pm 8.40	-3.70 \pm 3.70
11	-2.00 \pm 6.00	-4.00 \pm 4.00	-2.40 \pm 8.40	-3.70 \pm 3.70
12	7.00 \pm 6.00	20.00 \pm 4.00	-2.40 \pm 8.40	97.20 \pm 3.70	0.35	WN7
13	1.00 \pm 6.00	-2.00 \pm 4.00	3.20 \pm 8.40	1.90 \pm 3.70
14	1.00 \pm 6.00	-6.00 \pm 4.00	-2.40 \pm 8.40	-1.90 \pm 3.70
15	1.00 \pm 6.00	-8.00 \pm 4.00	-2.40 \pm 8.40	-3.70 \pm 3.70
16	1.00 \pm 6.00	-2.00 \pm 4.00	0.40 \pm 8.40	22.40 \pm 3.70
17	19.00 \pm 6.00	36.00 \pm 4.00	-10.80 \pm 8.40	202.00 \pm 5.60	0.53	WN7
18	4.00 \pm 6.00	-4.00 \pm 4.00	-5.20 \pm 8.40	-7.50 \pm 3.70
19	7.00 \pm 6.00	8.00 \pm 4.00	-2.40 \pm 8.40	80.40 \pm 3.70	0.88	WN6-7
20	1.00 \pm 6.00	-4.00 \pm 4.00	-2.40 \pm 8.40	9.40 \pm 1.90
21	7.00 \pm 6.00	24.00 \pm 4.00	-8.00 \pm 8.40	129.00 \pm 3.70	0.29	WN7-8
22	19.00 \pm 6.00	40.00 \pm 4.00	6.00 \pm 8.40	173.90 \pm 5.60	0.48	WN7
23	13.00 \pm 6.00	28.00 \pm 4.00	-8.00 \pm 8.40	144.00 \pm 3.70	0.46	WN7
24	16.00 \pm 6.00	34.00 \pm 4.00	-10.80 \pm 8.40	179.50 \pm 5.60	0.47	WN7
25	10.00 \pm 6.00	24.00 \pm 4.00	-8.00 \pm 8.40	136.50 \pm 3.70	0.42	WN7
26	7.00 \pm 6.00	16.00 \pm 4.00	-5.20 \pm 8.40	76.70 \pm 3.70	0.44	WN7
27	-8.00 \pm 6.00	0.00 \pm 6.00	-2.40 \pm 8.40	1.90 \pm 3.70
28	7.00 \pm 6.00	20.00 \pm 4.00	-8.00 \pm 8.40	130.90 \pm 3.70	0.35	WN7
29	1.00 \pm 6.00	2.00 \pm 4.00	-5.20 \pm 8.40	24.30 \pm 3.70	0.50	WN7
30	1.00 \pm 6.00	2.00 \pm 4.00	-5.20 \pm 8.40	29.90 \pm 3.70	0.50	WN7
31	-2.00 \pm 6.00	-4.00 \pm 4.00	-5.20 \pm 8.40	5.60 \pm 1.90
32	7.00 \pm 6.00	0.00 \pm 4.00	-5.20 \pm 8.40	-22.40 \pm 1.90
33	-8.00 \pm 6.00	-8.00 \pm 4.00	0.40 \pm 8.40	-7.50 \pm 1.90

Table 5—Continued

Star ID	He II 2.19 μm^{a}	Br γ ^a	He I 2.06 μm^{a}	P α^{a}	He II 2.19 $\mu\text{m}/\text{Br}\gamma$	SpTyp ^b
34	13.00 \pm 6.00	22.00 \pm 4.00	-8.00 \pm 8.40	119.70 \pm 5.60	0.59	WN7

^aEquivalent width is calculated as the narrow-band index multiplied by the filter bandpass; see §2.1.3

^bSpTyp from Figer et al. (1997) assuming the stars are Wolf-Rayet type (Cotera et al. 1996) and not Of supergiants; see text